Endoplasmic reticulum remains continuous and undergoes sheet-to-tubule transformation during cell division in mammalian cells

Maija Puhka, Helena Vihinen, Merja Joensuu, and Eija Jokitalo

Electron Microscopy Unit, Institute of Biotechnology, University of Helsinki, 00014 Helsinki, Finland

The endoplasmic reticulum (ER) is a multifaceted cellular organelle both structurally and functionally, and its cell cycle–dependent morphological changes are poorly understood. Our quantitative confocal and EM analyses show that the ER undergoes dramatic reorganization during cell division in cultured mammalian cells as mitotic ER profiles become shorter and more branched. 3D modeling by electron tomography reveals that the abundant interphase structures, sheets, are lost and subsequently transform into a branched tubular network that remains continuous. This is confirmed by observing the most prominent ER subdomain, the nuclear envelope (NE). A NE marker protein spreads to the mitotic ER tubules, although it does not show a homogenous distribution within the network. We mimicked the mitotic ER reorganization using puromycin to strip the membrane-bound ribosomes from the interphase ER corresponding to the observed loss of ribosomes normally occurring during mitosis. We propose that the structural changes in mitotic ER are linked to ribosomal action on the ER membranes.

Introduction

The endoplasmic reticulum (ER) is the largest and most multifunctional cellular organelle. It is composed of three structurally distinct subdomains, nuclear envelope (NE) enclosing the nucleus and rough and smooth ER that spread around the entire cytoplasm, contacting other organelles in several regions (Voeltz et al., 2002). The reticulum is composed of flattened sheets and tubules that branch to generate a polygonal network. The diameter of the tubules and the thickness of the sheets in the network are both about 60–100 nm.

ER plays a crucial role in synthesis, modification, transport, and degradation of membrane and secretory proteins, and is the site for biosynthesis, processing, and transport of several lipids, and for regulation of cytosolic calcium level (Sitia and Meldolesi, 1992). Considering the multitude of functions attributed to the ER, it is believed that the complexity of the ER is greater than the tripartite division suggests (Sitia and Meldolesi, 1992; Staehelin, 1997; Papp et al., 2003). Specialized subdomains have been suggested and in some cases shown to exist, but their composition and distribution is still mostly unclear (Geuze et al., 2003; Rizzuto et al., 2004; Robenek et al., 2004; Levine and Rabouille, 2005). Morphological aspects of the ER are very challenging to study because ER is a highly dynamic organelle that constantly rearranges its polygonal structure (Baumann and Walz, 2001). The first proteins involved in tubule generation, maintenance, and branch point generation, the reticulon and DP1 families and p22, have been identified (Andrade et al., 2004; Shibata et al., 2006; Voeltz et al., 2006), but sheet formation is still a mystery.

Little is known about the morphogenesis of the ER during cell division, or the partitioning of the NE or other functional subdomains in relation to, or within, the reticular ER in animal cells (Lowe and Barr, 2007). Although morphologically different in interphase, the distinction between the NE and the rest of the ER is less clear during cell division. Earlier models, which were mainly based on EM data, suggested complete fragmentation of the NE and fragmentation of the rest of the ER to a variable extent, yielding a heterogeneous population of fragments (Zeligs and Wollman, 1979; Warren and Wickner, 1996; Dreier and Rapoport, 2000; Du et al., 2004). On the other hand, FRAP experiments have shown that after the NE breakdown, proteins of the NE disperse into the ER, which remains continuous during cell division (Ellenberg et al., 1997). It is not known whether the NE proteins spread evenly throughout the ER, how subdomains within the reticular ER are partitioned, and how ER network organization itself changes during cell division.

There are few studies where changes in the overall structure of the ER during cell division have been systematically

Correspondence to Eija Jokitalo: eija.jokitalo@helsinki.fi

Abbreviations used in this paper: ET, electron tomography; LBR, lamin beta receptor; NE, nuclear envelope; TEM, transmission electron microscopy.

The online version of this paper contains supplemental material.

The Journal of Cell Biology, Vol. 179, No. 5, December 3, 2007 895–909
http://www.jcb.org/cgi/doi/10.1083/jcb.200705112

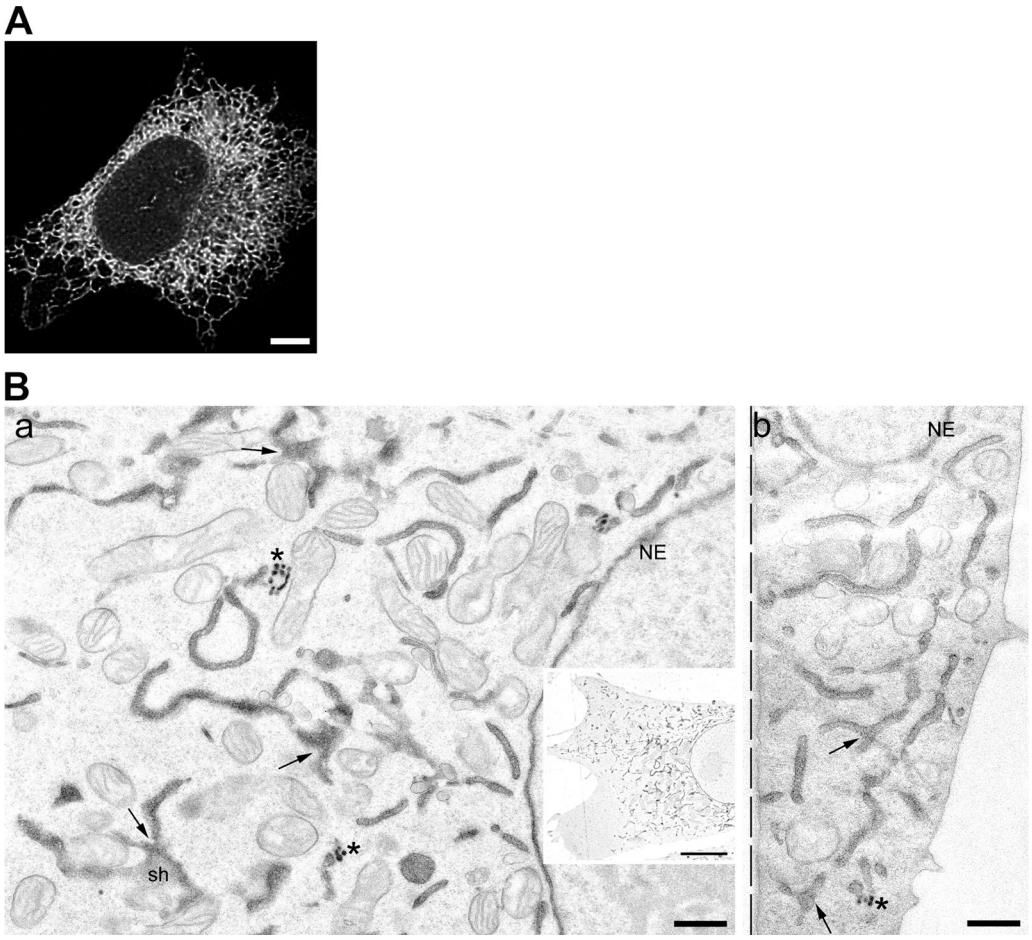

Figure 1. **Morphology and overall distribution of the interphase ER.** (A) A maximum intensity projection of a deconvoluted confocal stack of Hsp47-GFP/CHO-K1 cells showing that the ER network is denser in the perinuclear area of the cell. Bar, 5 μm. (B) Labeling with peroxidase cytochemistry in ssHRP-KDEL/CHO-K1 cells. Interphase cells sectioned parallel (a) or perpendicular to the coverslip (dashed line, b) have long ER profiles of tubules and sheets (sh). The ER branch points (arrows), exit sites (*), and NE are indicated. The small inset shows the overall distribution of the ER. Bars are 0.5 μm in high and 5 μm in low magnification images.

characterized, and it is evident that both structure and distribution of the ER within cells varies among different species and according to developmental stage or differentiation (Terasaki, 2000; Terasaki et al., 2001; Wollert et al., 2002; Bobinnec et al., 2003; McCullough and Lucocq, 2005; Poteryaev et al., 2005). These studies have shown that the ER undergoes dramatic changes during cell cycle reflecting the different needs of each cell type, and suggest that several mechanisms for partitioning have evolved. Study of cultured animal cells that have relatively simple signaling cascades and are unspecialized with respect of secretion or storage may reveal some basic fundamental mechanisms behind the partitioning of the ER and its subdomains.

In the present study, we analyzed the architecture of the ER in mammalian cells using a combination of light microscopy (LM) and EM techniques. We characterized the reticular ER in interphase and in dividing cells and the relation of NE and ER during cell division by quantitative morphometric assays, where tubule or cisternal length and the number of branch points were the two main features measured. We used two different approaches: confocal microscopy for live-cell visualization of the ER, and transmission electron microscopy (TEM) analysis of fixed cells to ensure higher resolution. In our TEM studies, we used thin sections for morphometric analysis, and for appreciation of the 3D structure, serial semi-thick sections were subjected to electron tomography (ET).

Our results show that the ER partitions as a continuous network and the NE partitions as part of the reticular ER. However, mitotic ER has a very different network structure compared to interphase ER. Morphometric assays revealed that it contains more branch points and shorter profiles than the interphase ER. By ET we were able to show that these changes in the network structure are accomplished by the transitioning of sheets into a tubular network. We provide mechanistic insight into the inheritance of the ER by showing that similar changes in the ER structure are induced by stripping of ribosomes with puromycin from the interphase ER. This is consistent with our observations on the decrease in ribosomes on the ER membranes during mitosis.

Results

Morphology of interphase ER is localization specific

We analyzed structure and distribution of the ER both at LM level using confocal microscopy and live cells, and then at

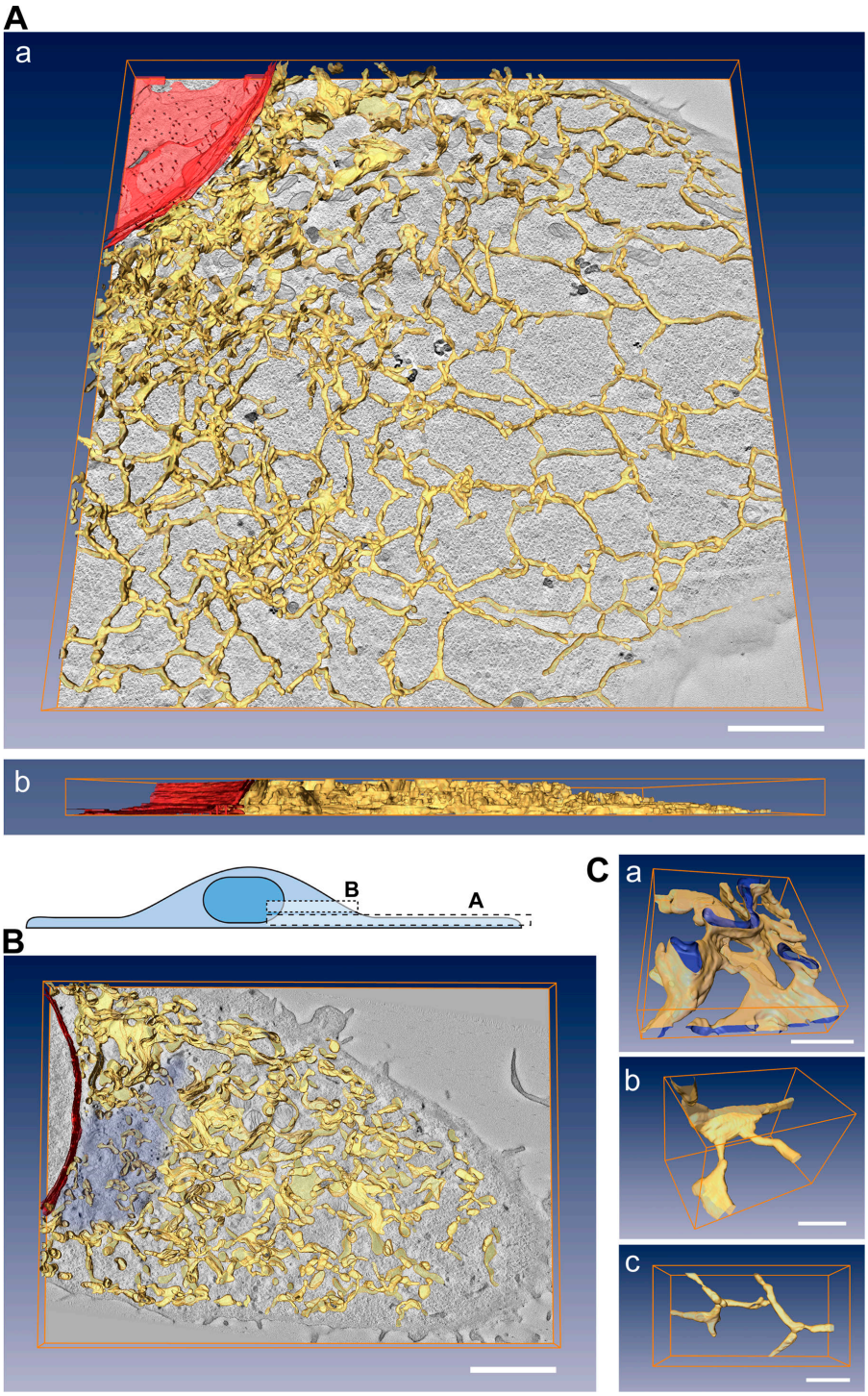

Figure 2. **Electron tomographic analysis of the interphase ER from two different cell depths.** (A and B) Three successive 200- or 250-nm thick sections from two ssHRP-KDEL/CHO-K1 cells were subjected to ET. The sections were the first ones from the bottom of the cell next to the coverslip (A) or from the middle of the cell depth (B) and show long interconnected tubules in the cell periphery and sheets in the more central parts of the cell (illustration demonstrates the cell depth where sections for imaging were selected). In A, (b) is a side view of the model in (a), and reveals the flat area of the lamellipodia. The ER is modeled in yellow and the NE in red. In B, the Golgi area is highlighted with darker gray. Bars, 2 µm. (C) Models of the different types of branch points between two sheets (a and Video 1), a sheet and a tubule (b), or two tubules (c). Bars, 500 nm.

higher resolution using EM. Stable cell lines were used to ensure better control over the expression level because transient expression is often too high and may yield structural artifacts (Ellenberg et al., 1997; Snapp et al., 2003; Ma et al., 2007).

For confocal microscopy, we used live CHO-K1 cells stably expressing luminal collagen-specific chaperone Hsp47 (Nagata, 1998) coupled to EGFP (Kano et al., 2005; Hsp47-GFP). Interphase ER appeared as a continuous network that was denser around the nucleus than at the periphery of the cells (Fig. 1 A). Tubules close to the plasma membrane, and especially at the leading edge of migrating cells, seemed longer than elsewhere.

We next observed the ER network at EM level. Here, we used CHO-K1 cell line stably expressing HRP coupled to the ER-targeting signal sequence and ER retention signal KDEL (Connolly et al., 1994; ssHRP-KDEL). This allowed cytochemical staining of the ER, and thus, precise identification of the ER membranes. Cells were cultured as a monolayer and fixed, stained, and embedded in Epon while still attached to glass coverslips in order to preserve natural cell shape (Jokitalo et al., 2001).

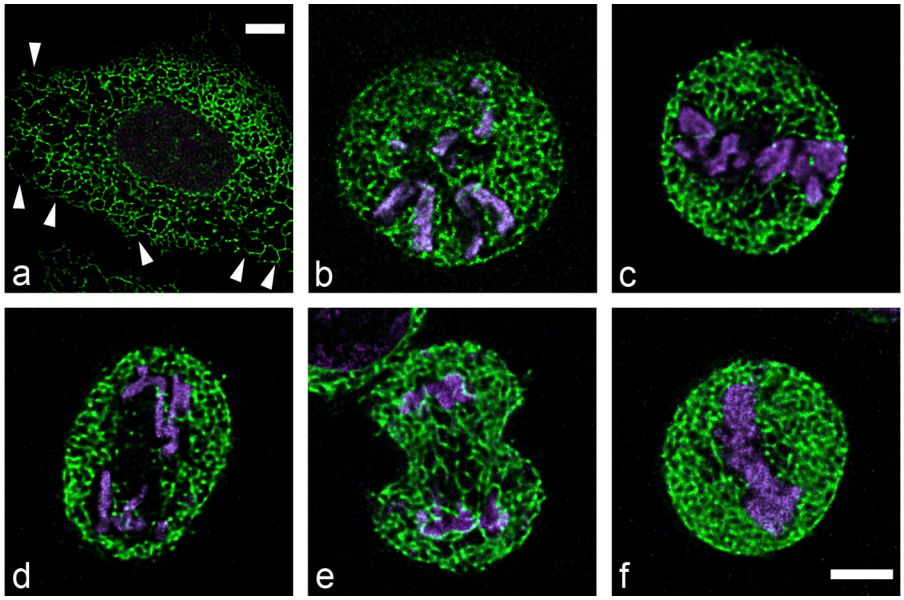

Figure 3. **Confocal microscopy analysis of the ER throughout the cell cycle.** Confocal optical sections of CHO-K1 cells expressing Hsp47-GFP (a–e) or ssGFP-KDEL (f) were obtained throughout the cell cycle. DNA was stained in vivo (in lilac). The ER of an interphase cell (a) shows a typical polygonal structure with denser network in the perinuclear area than in the periphery of the cells. Arrowheads indicate long tubules found in the cell periphery. In contrast to the interphase ER, the mitotic ER was denser and more evenly distributed. The spindle region excluding ER is visible in metaphase (c) and late anaphase (d) cells. The other phases shown are prometaphase (b), early telophase (e) and metaphase (f). Bars, 5 μm; bar in image f applies to images b–f.

In interphase cells, the staining was observed in ER tubules and sheets, ER exit sites (Bannykh et al., 1996), and the NE (Fig. 1 B, a and b). There were more ER profiles in the perinuclear area than in the cell periphery (low magnification image in Fig. 1 B, a).

When analyzing thin EM sections, one disadvantage is that cross-sections of sheets and tubules have similar profiles to tubules and vesicles, respectively. Therefore, the best way to appreciate the complex and pleiomorphic structure of the ER is to make 3D reconstructions by ET. For this, we imaged several relatively thick (200 or 250 nm) successive sections from cytochemically stained ssHRP-KDEL/CHO-K1 cells and produced models of ER by drawing the contours in the tomographic slices. Our models clearly demonstrated a continuity of the ER network in interphase cells. They also revealed the abundance of sheet structures that are otherwise difficult to observe by confocal microscopy or thin section EM. To study the impact of localization within the cell on the ER structure, we produced ER models from two different cell depths. A model derived from three bottom sections (illustration in Fig. 2, box A) demonstrates that the ER close to the plasma membrane as well as in the thin lamellipodia was composed of interconnected long tubules, and that sheets started to appear closer to the nucleus (Fig. 2 A, a and b). On the other hand, a model from the middle sections of the cell (illustration in Fig. 2, box B) showed abundant sheets in the central area of the cell and that tubules were mainly found in the periphery close to the plasma membrane and around the Golgi ribbon (Fig. 2 B). ET revealed three types of branch points, those between two sheets, a sheet and a tubule, or two tubules (Fig. 2 C, a–c; an animated model of sheet-to-sheet branch is included as Video 1, available at http://www.jcb.org/cgi/content/full/jcb.200705112/DC1).

ER undergoes morphological changes during cell cycle

We next analyzed the ER structure during different phases of the cell cycle. In all our experiments, we imaged naturally occurring mitotic cells in asynchronous cell populations. In confocal optical sections of mitotic cells (Fig. 3, b–e), ER resided at areas not occupied by the chromosomes and mitotic spindle and clearly retained the reticular form throughout mitosis. However, in contrast to interphase (Fig. 3 a), the network appeared denser and more evenly distributed.

These results were confirmed with a cell line stably expressing EGFP coupled to the ER-targeting signal sequence and ER retention signal KDEL (ssGFP-KDEL). This ER-marker gave similar results as Hsp47-GFP (a metaphase cell shown in Fig. 3 f).

At EM level, the mitotic ER profiles appeared short and fairly evenly distributed, although excluded from the spindle area (Fig. 4, a–d). ER exit sites quickly reduced in number after early prometaphase and emerged again during telophase.

In order to accurately characterize the global changes in the ER network during cell division, we quantified two parameters from live cells: ER profile lengths including tubular and cisternal profiles (referred to as ER profiles) and the number of branch points (three types; see Fig. 2 C), which is a direct indicator of network formation (Lee and Chen, 1988; Waterman-Storer and Salmon, 1998; Dreier and Rapoport, 2000; Uchiyama et al., 2002). Confocal section stacks spanning cells were deconvoluted to subtract background noise, and the ER network was then converted into a skeleton model (Fig. 5 A, a–c; one optical section shown). The skeleton is a one-pixel-thick 2D model of the network in an optical section and allows direct measurement of the above parameters and their relation to the area occupied by the ER (ER area) in the same section. To obtain a reliable average value for each cell, we selected three to five sections at regular intervals to cover the whole cell depth. The minimum length of the ER profiles was set to 0.2 μm, which is the theoretical resolution limit of the diffraction limited LM.

The average number of branch points in interphase Hsp47-GFP/CHO-K1 cells was 84 per 100 μm^2 ($\pm$12, n = 11 cells; Fig. 5 B, Table I). In mitotic cells, there were well over 100 branch

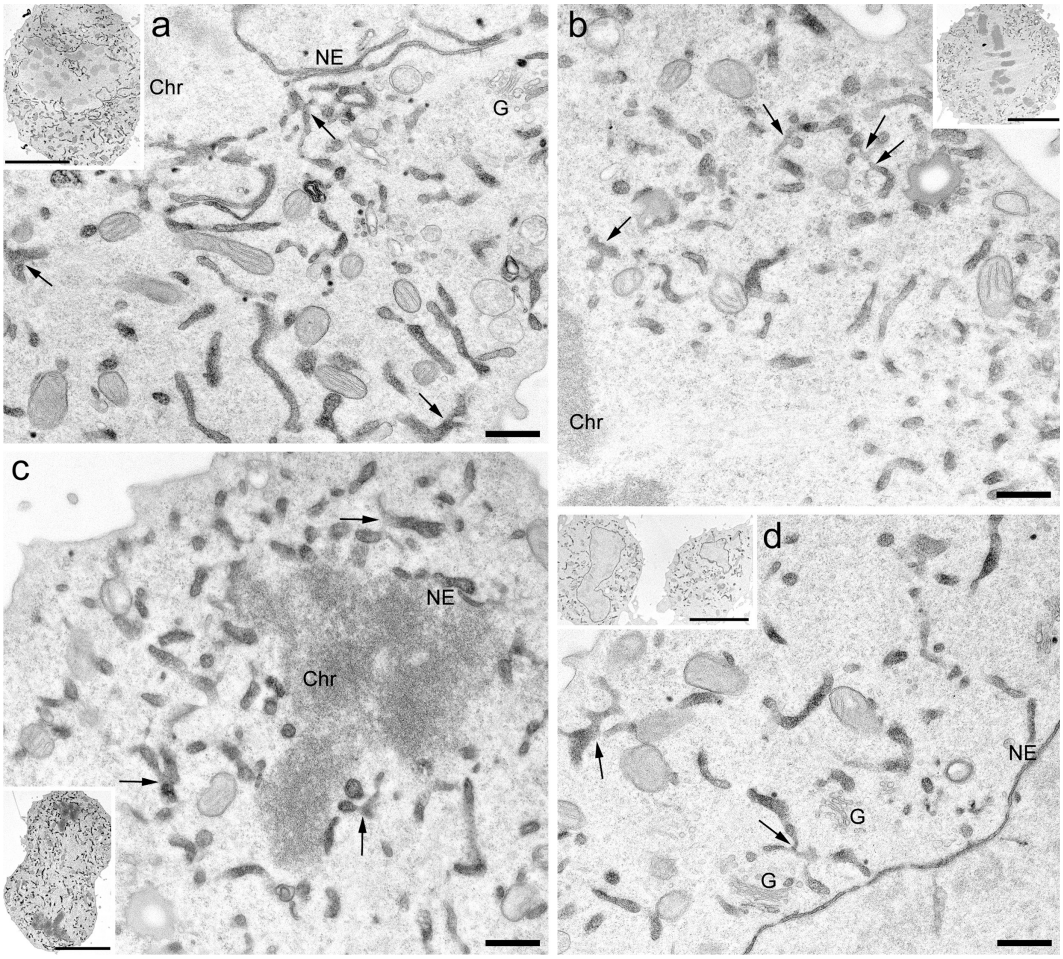

Figure 4. **Labeling of the ER network with peroxidase cytochemistry in mitotic ssHRP-KDEL/CHO-K1 cells.** The ER network lacks long ER profiles in prometaphase (a), metaphase (b), late anaphase (c), and telophase (d) cells, and has many branch points especially during metaphase. The small insets show the cell cycle phase and the overall distribution of the ER profiles. ER branch points (arrows), mitotic Golgi clusters (G), chromosomes (Chr) and NE are indicated. Bars are 0.5 μm in high and 5 μm in low magnification images.

points per 100 μm^2. The increase was especially high in metaphase cells, showing 36% increase (115 ±13, $n = 9$). During earlier and later phases of mitosis, the increase ranged between 23 to 27% (104–107 branch points per 100 μm^2). Similarly to the branch points, the total number of ER profiles was higher in mitotic cells than in interphase cells (Table I). Whereas interphase cells had 115 profiles per 100 μm^2 (±12, $n = 11$) on average, the number increased to 138 and 136 profiles during early and late mitosis, respectively, and reached the average top value of 142 profiles (±14, $n = 9$) during metaphase. Distribution of profiles in different length groups indicated that the change was mainly due to increased number of short ER profiles in mitotic cells (Fig. 5 C, Table I). In the shortest category (0.2–0.4 μm), there were 26% more profiles in early mitotic, 31% in metaphase, 20% in anaphase, and 14% in telophase cells. In the next length groups of 0.4–0.8 μm and 0.8–1.5 μm, the increase in the number of profiles during all mitotic phases was between 22–30% and 13–25%, respectively. There were no significant changes in the longest profile category (>1.5 μm).

The quantification of ssGFP-KDEL–positive ER showed 36% increase in branch points in metaphase (132 ± 20, $n = 5$) as compared to interphase cells (97 ± 10, $n = 3$). In other phases of mitosis the change from the interphase was not as high as with the other marker protein. The number of ER profiles changed only during metaphase, in which there was an increased number of short profiles (unpublished data).

Because the shape of the CHO-K1 cells changes from flat at interphase to round during cell division, we investigated whether the cell volume available for the ER diminishes, therefore forcing the network into denser configuration during mitosis. Our measurements from confocal section stacks showed that the cell volume was similar in interphase and mitotic cells. Interphase ER was confined to 80% of the cell volume, leaving 20% to the nucleus (±6%, $n = 7$). This ratio did not change in mitotic cells, being 78% for the ER and 22% for the chromosomes and mitotic spindle (±8%, $n = 22$). Thus, the ER takes up a similar volume of the cell throughout the cell cycle despite the changes in cell shape.

The morphometric analysis of the EM images confirmed the confocal microscopy results. The extent of ER network formation as measured by the number of branch points per ER area increased 39% from interphase (102 ± 26, $n = 22$) to metaphase

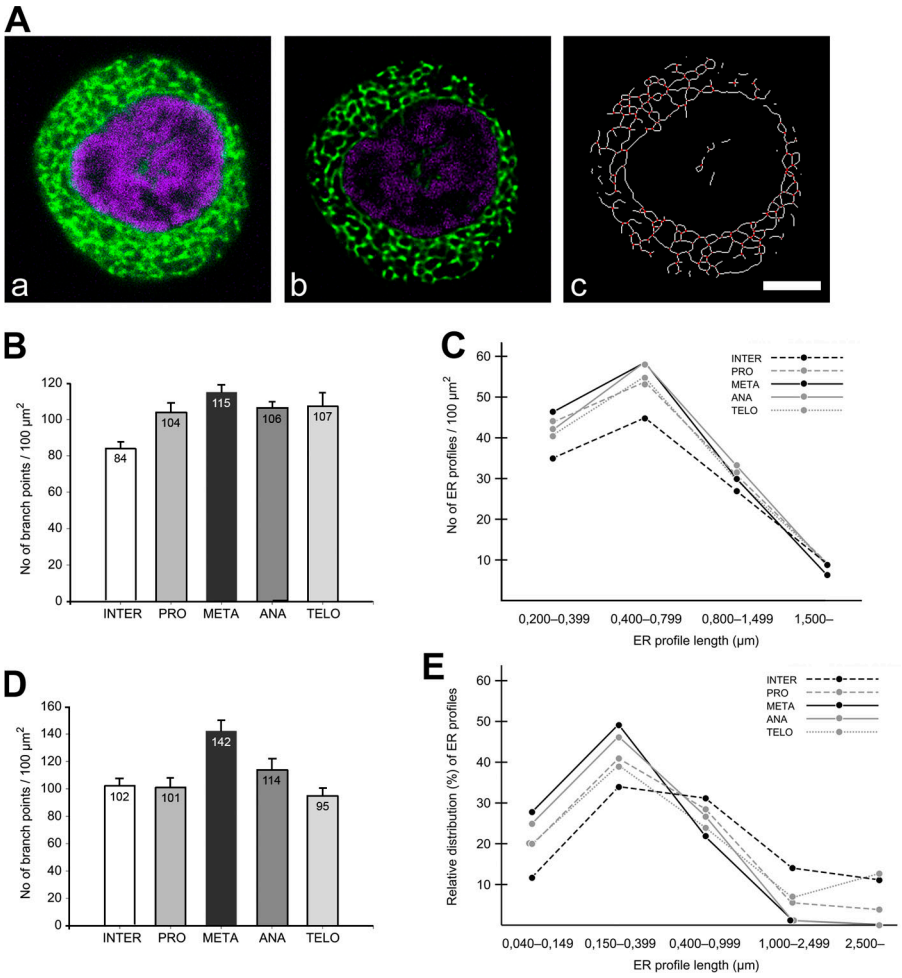

Figure 5. **Morphometric analysis of ER branch points and profile lengths.** Quantification was done from confocal images of Hsp47-GFP (B and C) and from EM images of ssHRP-KDEL (D and E) expressing cells. (A) Stacks of optical sections (a, prophase section shown) were deconvoluted (b) and a skeleton model (c) of the ER network was formed by ImagePro software showing branch points in red and ER profiles in white. Bar, 5 μm. (B) The number of branch points per ER area increased during mitosis and reached a peak value in metaphase. The branch point numbers were statistically different from the interphase values ($P < 0.01$) in all phases of mitosis. (C) Mitotic cells showed a clear increase in short 0.2–0.4 and 0.4–0.8 μm ER profiles ($P < 0.05$ except for telophase 0.2–0.4 μm) as compared to interphase cells. INTER = interphase ($n = 11$ cells), PRO = prophase to prometaphase ($n = 16$), META = metaphase ($n = 9$), ANA = anaphase ($n = 9$), TELO = telophase ($n = 7$). (D) The number of branch points per ER area increased from interphase to metaphase and returned to the interphase level after mitotic exit. The branch point number in metaphase was statistically different from the interphase value ($P < 0.001$). (E) Mitotic cells had a significantly increased proportion of short ER profiles (0.040–0.400 μm) and reduced proportion of long profiles (>1.000 μm) as compared to interphase cells ($P < 0.001$). This pattern was most pronounced in metaphase cells. INTER ($n = 22$), PRO ($n = 18$), META ($n = 15$), ANA ($n = 14$), TELO ($n = 18$). The values are presented as the mean ± SEM.

(142 ± 31, $n = 15$) and dropped back to the interphase level upon mitotic exit (Fig. 5 D, Table II). Dividing cells had considerably larger number of short profiles and smaller number of long profiles than interphase cells. The change was most pronounced during metaphase, when the increase in short profiles outnumbered the decrease in long profiles such that the total ER profile number per ER area was increased approximately 70%. The sum of the lengths of all ER profiles per ER area, however, remained equal, 112 ± 15 μm per 100 μm^2, at all phases of the cell cycle, and showed similar standard deviation within individual mitotic phase groups than between them (Table II).

The distribution of ER membranes in different length categories revealed that the two shortest groups had the highest number of profiles throughout the cell cycle and changed most during mitosis (Fig. 5 E, Table II). The largest proportion of profiles was taken up by the group of 0.150–0.400 μm profiles: 33% during interphase, around 40% in the groups of prophase and prometaphase and telophase, and more than 45% during meta- and anaphase. The increase in short ER profiles was balanced by decrease in long ER profiles. The largest decrease was observed in long 1.000–2.500-μm profiles: their proportion was reduced by more than 90% during metaphase and anaphase. As expected, the longest profiles starting from 2.500 μm and consisting almost entirely of the NE profiles were absent during meta- and anaphase and close to the interphase level during telo- and prophase. These results indicate that ER membranes are

Table I. **Change in the number of ER profiles and branch points during cell cycle in confocal optical sections of live cells**

	INTER	PRO	META	ANA	TELO
Branch points	84 ± 12	104 ± 20	115 ± 13	106 ± 10	107 ± 20
Total profiles	115 ± 12	138 ± 16	142 ± 14	143 ± 9	136 ± 16
0.200–0.399 μm	35 ± 5	44 ± 9	46 ± 4	42 ± 6	40 ± 8*
0.400–0.799 μm	45 ± 5	54 ± 7	58 ± 7	58 ± 6	55 ± 10
0.800–1.499 μm	27 ± 4	31 ± 3	30 ± 6*	33 ± 3	31 ± 5
≥1.500 μm	9 ± 2	9 ± 2*	7 ± 1*	9 ± 1*	9 ± 2*

The numbers are presented as the mean value per 100 μm^2 of ER area ± SD. The values in all mitotic groups were statistically different from interphase ($P < 0.05$), except in those marked with *. INTER = interphase ($n = 11$ cells), PRO = prophase to prometaphase ($n = 16$ cells), META=metaphase ($n = 9$ cells), ANA = anaphase ($n = 9$ cells), TELO = telophase ($n = 7$ cells).

converted from long membrane structures into a large number of shorter highly branched structures in mitotic cells.

Denser ER network is accomplished by transformation of sheets to tubules

What kind of morphological changes can explain the increased numbers of branch points and short profiles in the mitotic ER? To elucidate this, corresponding tomographic models from interphase and dividing cells were done from upper middle sections (see illustration in Fig. 6 D) covering perinuclear area to plasma membrane in interphase cells and an area including some of the condensed chromosomes and reaching to the plasma membrane in dividing cells. In the modeled area of an interphase cell (Fig. 6 A), most of the ER appeared as sheets and only few tubular ER structures were found. Similar sheet structures were found in the tomogram of specimen sectioned perpendicular to the coverslip (Fig. 6 B). Some of the sheets with low curvature extended through the whole tomographic volume (800 nm, an animated model of interphase ER is included as Video 2, available at http://www.jcb.org/cgi/content/full/jcb.200705112/DC1).

On the other hand, a modeled metaphase ER illustrated the dramatic changes in structure as it nearly completely lacked sheets (Fig. 6 C; an animated ER model of a metaphase cell is included as Video 3, available at http://www.jcb.org/cgi/content/full/jcb.200705112/DC1). ET revealed that mitotic ER is mostly tubular in structure, and that this tubular network remains continuous. Similar results, continuous tubular network with greatly reduced sheet structures, were obtained from a modeled ER of an anaphase cell (unpublished data). Thus, 3D ET analysis showed the continuity of ER during different phases of the cell cycle and indicated the morphological transformation from sheet structures of interphase cells into tubular structures in dividing cells.

Partitioning of the NE is subordinate to the ER network

In order to follow the fate of the NE during mitosis, we created CHO-K1 cell lines stably expressing the inner nuclear membrane marker lamin ß receptor coupled to EGFP (LBR-GFP; Ellenberg et al., 1997) or HRP. In both cases, we chose a clone that had a low expression level to avoid abnormal structures of the NE and leaking of the marker into the peripheral ER during interphase (Ellenberg et al., 1997; Ma et al., 2007). First, we re-examined the dispersal of the NE marker during cell division by live cell video and confocal microscopy. The video of four dividing LBR-GFP expressing cells (Video 4, available at http://www.jcb.org/cgi/content/full/jcb.200705112/DC1) shows how the marker is tightly kept on the NE during interphase and is redistributed to the reticular ER during cell division (cell 3 shown in Fig. S1, available at http://www.jcb.org/cgi/content/full/jcb.200705112/DC1) in agreement with the videos shown earlier using the same marker protein expressed in Cos7 cells (Ellenberg et al., 1997). During the mitotic NE dispersal, the fluorescent pattern became very faint. We attempted to quantify the structural changes of the LBR-GFP–positive membranes during mitosis using the method applied to Hsp47-GFP–expressing cells, but good skeleton models were not obtained because of the low expression level. Therefore, we continued the analysis using EM and peroxidase cytochemical staining of the LBR-HRP/CHO-K1 cell line. The NE of interphase cells was darkly stained, whereas the rest of the ER remained unstained (Fig. 7 a). During prophase, the staining still appeared on the NE, although stained ER profiles were occasionally seen outside the NE (Fig. 7 b and close-up of boxed area in Fig. 7 c). As the NE breakdown started (Fig. 7 d) and progressed further (Fig. 7 e), the number of stained profiles outside the NE increased and conversely, the NE staining became weaker. The NE formed long, still thin and often layered membrane stretches that surrounded the chromosomes. The membranes also retained some nuclear pores even after the NE had been perforated at several points (Fig. 7, d and e). After the NE breakdown and until late anaphase, LBR staining seemed to be distributed all over the reticulum (Fig. 7, e–g). However, a closer look revealed that the majority of the cells had both unstained and stained ER profiles (Fig. 7, f and g).

The behavior of the LBR label during late anaphase or early telophase was essentially the reversal of early mitosis: the label accumulated on the reforming NE and was retained there (Fig. 7, g and h). The NE seemed to be rebuilt directly from bits of the surrounding reticulum and established its thin NE-like

Table II. **Change in the number of branch points, total length, and relative length distribution of ER profiles in electron micrographs during cell cycle**

	INTER	PRO	META	ANA	TELO
Branch points	102 ± 26	101 ± 30*	142 ± 31	114 ± 30*	95 ± 23*
Total length (μm)	116 ± 14	106 ± 15*	115 ± 13*	111 ± 13*	111 ± 19*
0.040–0.149 μm (%)	12 ± 3 (154 ± 44)	20 ± 7 (225 ± 82)	28 ± 3 (360 ± 54)	25 ± 6 (311 ± 82)	20 ± 4 (233 ± 36)
0.150–0.399 μm (%)	33 ± 4 (153 ± 22)	41 ± 7 (179 ± 36)	49 ± 3 (234 ± 30)	47 ± 4 (215 ± 33)	39 ± 6 (177 ± 30)
0.400–0.999 μm (%)	31 ± 5 (61 ± 10)	28 ± 5* (53 ± 13)	22 ± 4 (48 ± 12)	27 ± 7* (53 ± 15)	24 ± 4 (47 ± 10)
1.000–2.499 μm (%)	14 ± 5 (11 ± 5)	6 ± 6 (5 ± 5)	1 ± 1 (1 ± 1)	1 ± 1 (1 ± 1)	7 ± 5 (5 ± 4)
≥2.500 μm (%)	11 ± 5 (3 ± 2)	4 ± 5 (1 ± 1)	0 ± 0 (0 ± 0)	0 ± 0 (0 ± 0)	12 ± 9* (3 ± 2)*

The branch points and the total length of ER profiles are presented as the mean value per 100 μm^2 of ER area ± SD. Relative length distribution of ER profiles are presented as the proportion (%) of each category ± SD, and the number of ER profiles per 100 μm^2 of ER area in each length category ± SD is shown in parentheses. The values in all mitotic groups were statistically different from interphase ($P < 0.05$), except in those marked with an asterisk. INTER = interphase (n = 22 cells), PRO = prophase to prometaphase (n =18 cells), META = metaphase (n = 15 cells), ANA = anaphase (n = 14 cells), TELO = telophase (n = 18 cells).

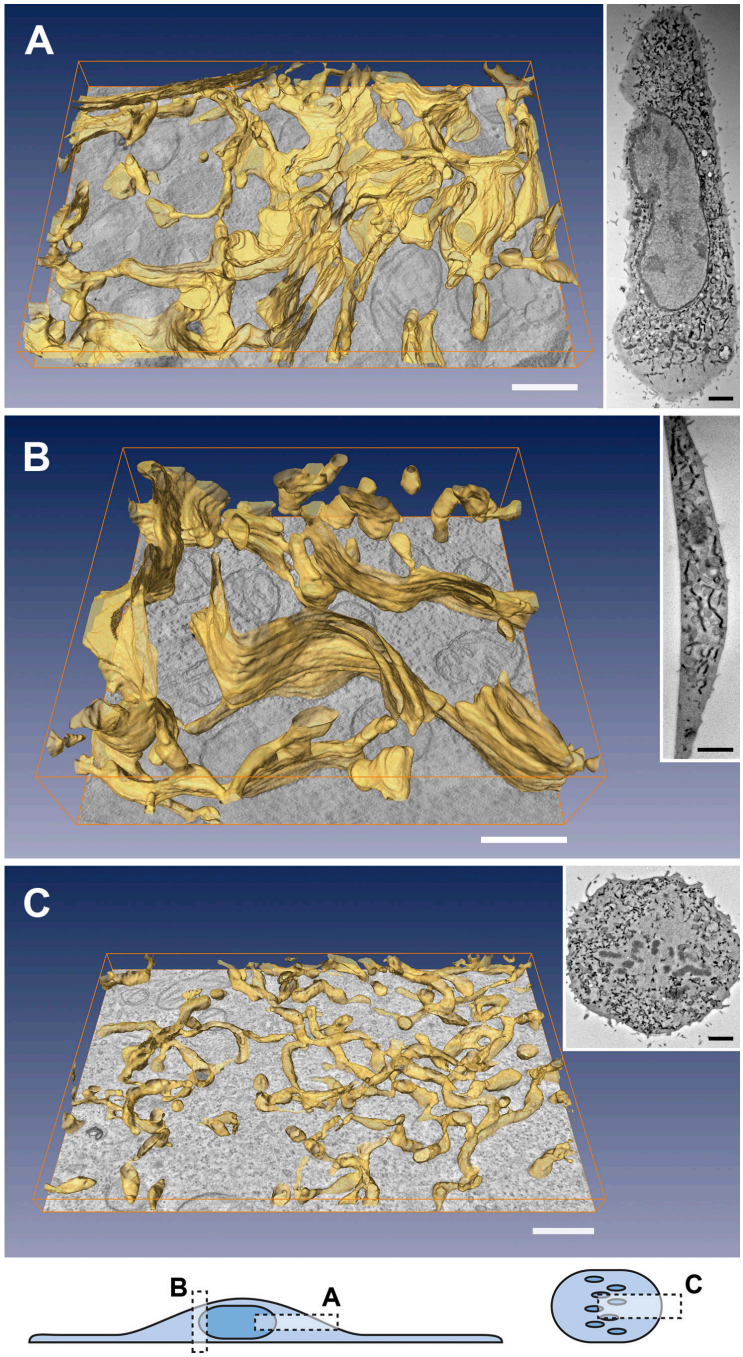

Figure 6. **Electron tomographic analysis of the ER in interphase and metaphase cells.** Successive semi-thick sections (200 nm) from ssHRP-KDEL/CHO-K1 cells were subjected to ET. The modeled ER in the interphase cell appeared mostly as sheets both in sections cut parallel (A, combined from 3 sections) and perpendicular (B and Video 2, combined from 4 sections) to the coverslip. The structure of the ER in metaphase cell appeared tubular and lacked sheets (C and Video 3, combined from 2 sections). The insets are EM micrographs at low magnification to indicate the phase of the cell cycle. The illustration shows the depth of the modeled volume of cells. Note that A and B are from separate cells. Bars are 500 nm, and in insets 2 μm.

appearance only after sufficiently long membranes had formed on the chromosome surface.

Next, the structure of NE during cell division was further analyzed by ET. For this, we used the same stable LBR-HRP/CHO-K1 cell line and ET was implemented as previously described to the corresponding areas from upper middle sections of the cell (illustration in Fig. 6). After the NE breakdown during prometaphase, the remnants of the NE could be seen as heavily stained profiles (see arrowheads in Fig. 8 A, inset). In a 3D model, these membranes appeared as small sheet structures that were thinner than the reticular ER and had still nuclear pores. A part of the reticular ER at this phase clearly appeared unstained. After the cell division progressed, the NE could no longer be morphologically distinguished, and the LBR-HRP was dispersed into the reticular ER (Fig. 8 B). During metaphase, the 3D structures of both LBR-HRP– and ssHRP-KDEL–marked ER membranes were indistinguishable from each other (Figs. 8 B and 6 C, respectively). In a telophase cell, the condensed chromosomes seemed to be surrounded by heavily stained NE membranes (Fig. 8 C, colored in red) that could occasionally be discerned already in anaphase cells (unpublished data). The small, thin sheet structures appeared to have nuclear pores (not seen in the picture). In all phases of cell division, the distribution of LBR-HRP was non-homogeneous, and the stained ER tubules were directly continuous with the unstained ones. The modeled ER network totally lacked sheet structures during metaphase (Fig. 8 B)

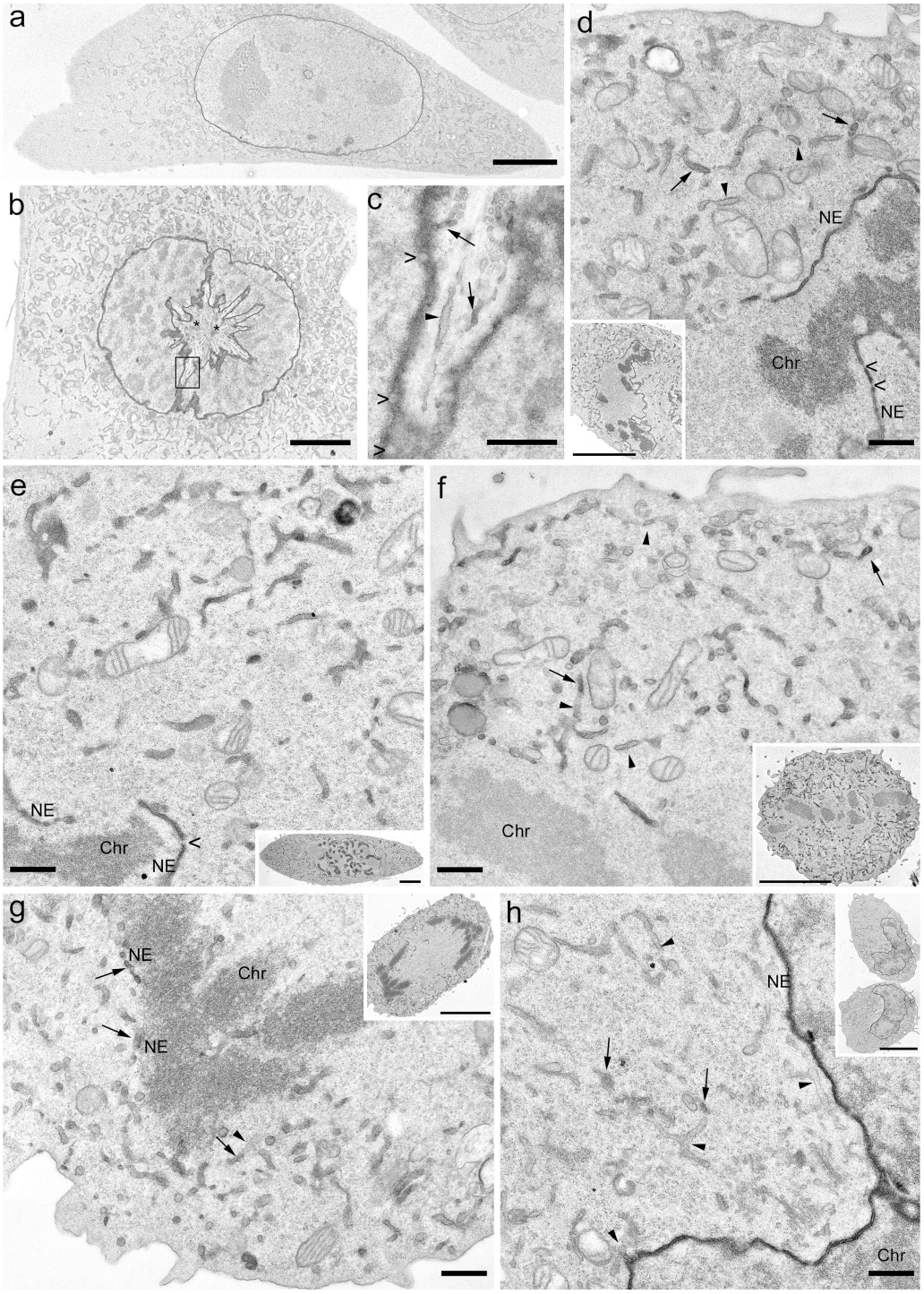

Figure 7. **EM analysis of the NE throughout the cell cycle.** Cytochemically stained LBR-HRP/CHO-K1 cells during interphase (a) and early prophase (b, boxed area enlarged in c), prometaphase (d and e), metaphase (f), anaphase (g), and telophase (h). The NE marker dispersed to the reticular ER after the NE breakdown and started to accumulate back to the reforming NE during late anaphase. Unstained ER tubules (arrowheads) were frequently observed next to or continuous with stained ER tubules (arrows) during all phases of mitosis. Cross-sections of nuclear pores (open arrows), chromosomes (Chr), NE, and centrioles (*) are indicated. Bars are 0.5 μm in high (c, d–h) and 5 μm in low magnification images.

and at later phases during cell division the only sheet structures found were the ones surrounding the condensed chromosomes (Fig. 8 C). Thus, the NE seemed to lose its identity during cell division while becoming a part of the ER network and thereby, the partitioning of the NE is subordinated to the ER network during cell division.

Dissociation of membrane bound ribosomes induces tubulation of ER and loss of sheets

What is behind the loss of ER sheets during mitosis? In a recent review on sheets and tubules, an idea of polysomes and their associated proteins acting as sheet stabilizers was presented

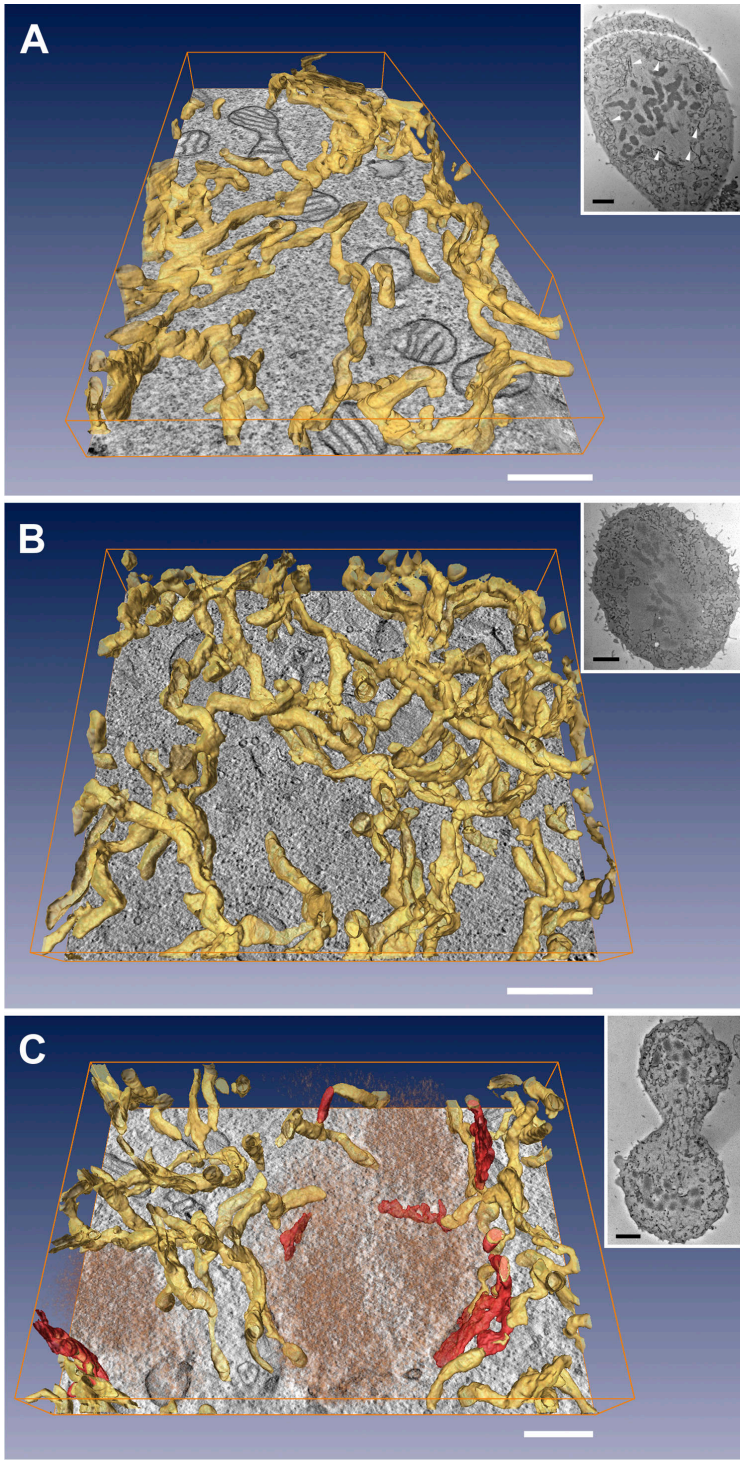

Figure 8. **Electron tomographic analysis of the NE in mitotic cells.** Successive semi-thick sections (200 or 250 nm) from LBR-HRP/CHO-K1 cells were subjected to ET. (A) In the prometaphase cell, the modeled ER (combined from 3 sections) showed mostly tubular structure, however, the remnants of the NE could be observed as darkly stained profiles (arrowheads in inset A). (B) During metaphase, the NE marker protein could be found dispersed in the tubular ER network (combined from 3 sections). (C) The telophase ER still had mostly tubular structure (combined from 4 sections), although the NE marker started to accumulate in the small sheet structures around the chromosomes. ER is modeled in yellow, darkly stained membranes in red, and chromosomes in light brown. The insets are EM micrographs indicating the cell cycle phase. Bars are 500 nm, and in insets 2 μm.

(Shibata et al., 2006). Furthermore, it is known that translation is inhibited in large part and polysomes break down during mitosis (Scharff and Robbins, 1966; Le Breton et al., 2005). To test this hypothesis, we first quantified ER-bound ribosomes from interphase and mitotic CHO-K1 cells. Thin-section EM images were obtained from the perinuclear area of interphase cells, where most sheets are found, and corresponding areas were imaged from prometaphase to early anaphase cells (see illustration in Fig. 6; Fig. 9 A, a and b). Interphase cells had 12.5 ribosomes/μm of transversely sectioned ER membrane (±2.3, n = 14 cells or total of 5,060 ribosomes per 405 μm of ER membrane), whereas mitotic cells had only 3.7 ribosomes/μm (±0.7, n = 17 cells or total of 2,811 ribosomes per 777 μm of ER membrane; 70.4% decrease).

We next simulated the mitotic translational inhibition by treating CHO-K1 cells with puromycin or cycloheximide. Both drugs inhibit translation, but only puromycin is known to quickly dissociate polysomes from ER membranes. Cycloheximide, in

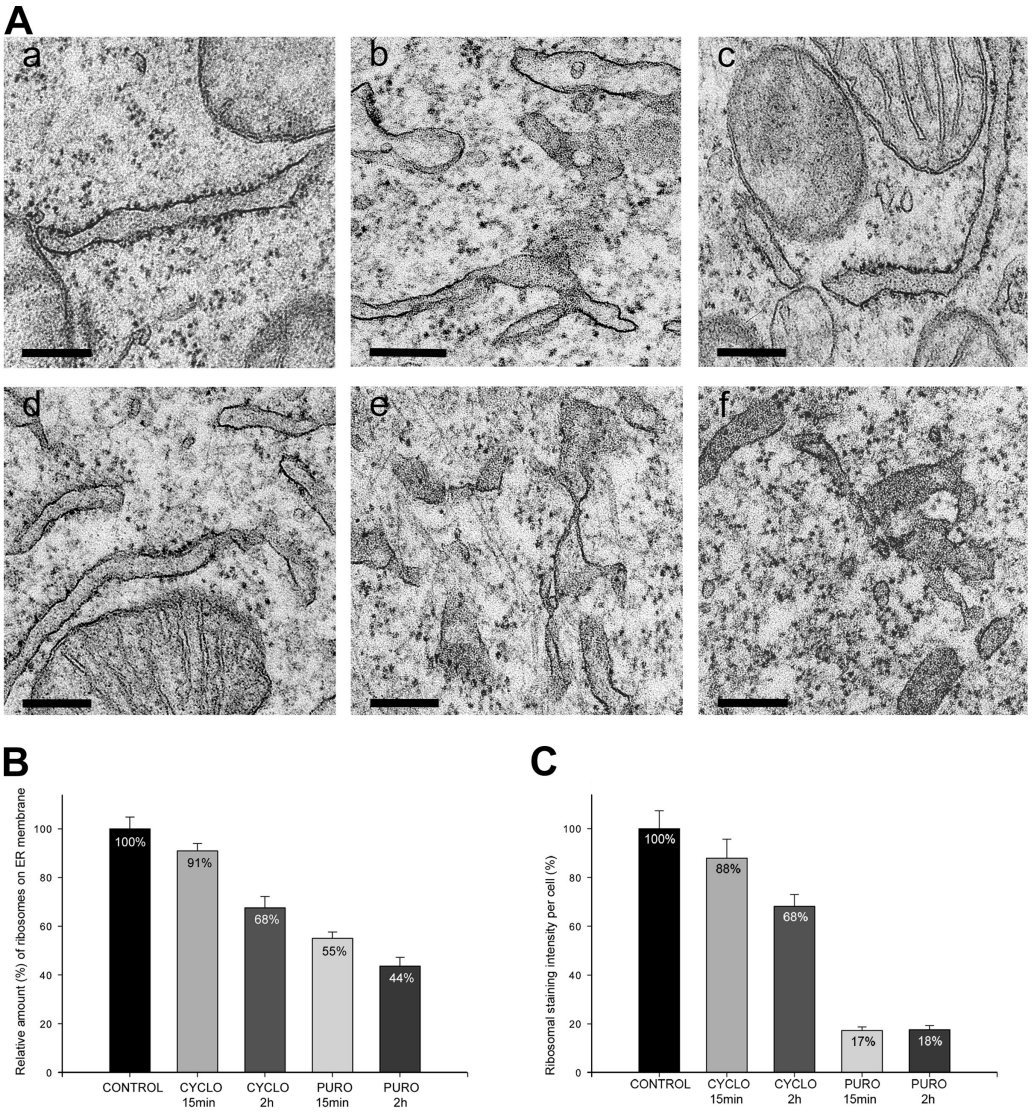

Figure 9. **Comparison of ER-bound ribosomes in untreated interphase or mitotic, and cycloheximide or puromycin treated interphase CHO-K1 cells.** (A) Thin-section EM analysis of untreated interphase (a) and mitotic prometaphase to early anaphase (b) cells, and interphase cells treated with cycloheximide (c and d) or puromycin (e and f) for 15 min or 2 h, respectively. Analysis revealed ER membranes covered with ribosomes in untreated and 15-min cycloheximide-treated interphase cells, whereas the ER in mitotic, puromycin treated and 2-h cycloheximide-treated cells had reduced number of ribosomes. Bars, 200 nm. (B) Relative amount of ribosomes on ER membrane quantified from thin-section EM images. (C) The small ribosomal subunit protein S6 was stained in semi-permeabilized salt-washed Hsp47-GFP/CHO-K1 cells for immunofluorescence analysis. Results are expressed as relative staining intensity per cell. In B and C, the values are presented as the mean ± SEM ($P < 0.001$ in cycloheximide [cyclo] 2 h, and puromycin [puro] 15 min and 2 h).

contrast, stabilizes ribosomal association with translocons (Seiser and Nicchitta, 2000; Roy and Wonderlin, 2003). A treatment of interphase cells for 15 min with cycloheximide did not change the ER morphology (Fig. 10 A). ET showed sheets and tubules connected to each other as in non-treated cells. ER-bound ribosomes were also normally present, 11.4 ribosomes/μm (±1.5, $n = 15$ cells; 8.8% decrease; Fig. 9 A, c and Fig. 9 B). In contrast, a similar 15-min treatment of cells with puromycin lead to a marked tubulation and perforation of ER sheets as seen clearly in 3D reconstruction (Fig. 10 B). The puromycin-treated interphase ER resembled mitotic ER; tubular profiles were increased and any remaining sheets were either very small or extensively perforated. However, tubules outside the perforated sheets seemed longer than average mitotic tubules. Analysis of thin sections revealed smooth ER membranes with markedly reduced number of ribosomes, 6.9 ribosomes/μm (±1.2, $n = 15$ cells; 44.8% decrease; Fig. 9 A, e and Fig. 9 B). A prolonged 2-h puromycin treatment of interphase cells gave similar results, although the number of ribosomes on ER membranes was further reduced to 5.5 ribosomes/μm (±1.2, $n = 9$ cells; 56% decrease; Fig. 9 A, f and Fig. 9 B). Interestingly, a 2-h treatment with cycloheximide caused tubulation and perforation of ER sheets that was not seen after the shorter incubation time (ET data now shown). However, similarly to the puromycin samples, the amount of membrane-bound ribosomes was reduced to 8.5 ribosomes/μm (±1.8, $n = 9$ cells; 32% decrease; Fig. 9 A, d and Fig. 9 B). This is consistent with previous data showing that with longer incubation time or at higher concentration, cycloheximide also causes

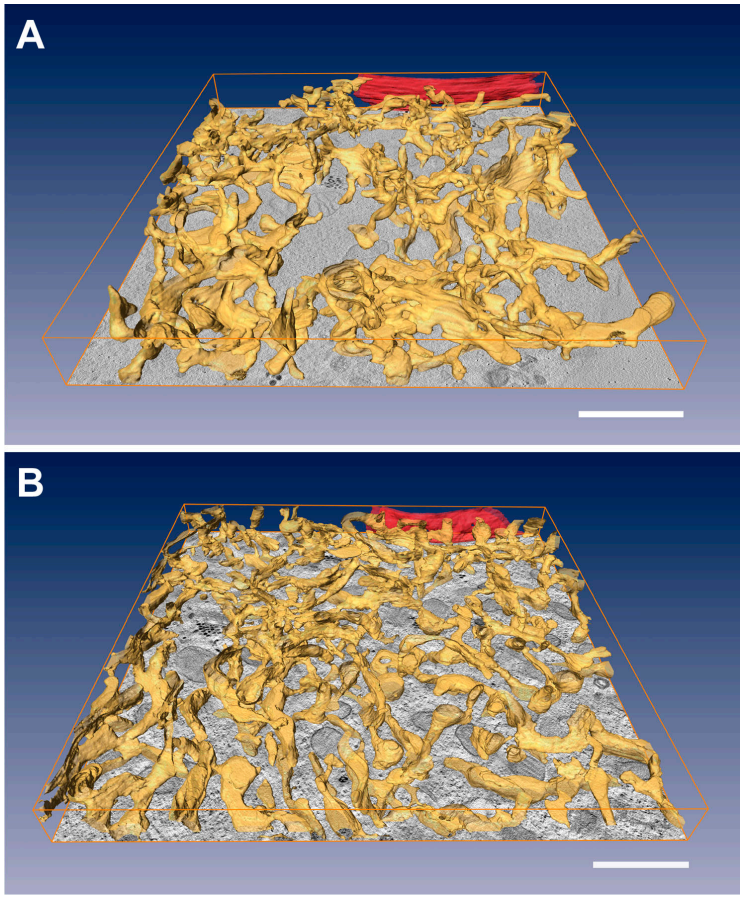

Figure 10. **ET analysis of cycloheximide- or puromycin-treated interphase cells.** The interphase ER (yellow) was modeled from three successive sections (250 nm) of ssHRP-KDEL/CHO-K1 cells treated for 15 min either with cycloheximide (A) or puromycin (B). The ER in cycloheximide-treated cell was composed of tubules and sheets whereas puromycin-treated cell had only tubular ER. The NE is modeled in red. Illustration in Fig. 2 (box B) demonstrates the cell depth where sections for imaging were selected. Bars, 1 μm.

stripping of ribosomes from the membranes (Van Coppenolle et al., 2004).

Puromycin has been shown to break down the ribosome, that is, the 40S subunit dissociates first and leaves the 60S subunit bound to the translocon (Seiser and Nicchitta, 2000). In EM images, the presence or the absence of the small ribosomal subunit cannot be reliably discerned. Therefore, the quantification of ribosomal detachment was confirmed and further investigated at LM level by staining the Hsp47-GFP/CHO-K1 cells with an antibody against the small ribosomal subunit protein S6. After the drug treatments, cells were semi-permeabilized and salt washed to remove the majority of the free cytosolic ribosomes before the staining of ER bound ribosomes. The co-localization of S6-staining and Hsp47-GFP was indicative of co-compartmentalization as shown by confocal microscopy: in untreated cells it was 59 ± 4% for Hsp47-GFP and 58 ± 6% for S6 ($n = 5$ cells) and similar numbers were obtained after the 15-min cycloheximide treatment (60 ± 5% and 54 ± 8%, $n = 4$ cells). Comparisons of the total intensities between control cells (set to 100%, $n = 60$ cells) and the treatment groups showed detachment of the small ribosomal subunit in cycloheximide-treated cells in agreement with the EM data after the 15-min and 2-h incubations (12% and 32% decrease, $n = 64$ and 71 cells, respectively; Fig. 9 C). In contrast, the detachment after the 15-min and 2-h puromycin treatments was greater (83% and 82% decrease, $n = 56$ and 63 cells, respectively; Fig. 9 C) than seen at EM level, as expected. These data suggest that ribosomes play a role in stabilizing flat sheet morphology because sheets are lost whenever ER-bound ribosomes decrease in number.

Discussion

Partitioning of the ER during cell division has been modeled and studied with numerous methods and cell types. The results have ranged from complete fragmentation of the ER to no fragmentation at all, giving support to stochastic or ordered inheritance models, respectively (Warren and Wickner, 1996; Du et al., 2004). Although the partitioning strategy varies between different cell types, controversial results may also reflect shortcomings of the investigation methods used. Elaborate ultrastructure, the dynamic nature of the ER, and cell shape changes during mitosis cause problems that cannot be overcome by a single method. Therefore, we chose to study cell cycle–dependent structural changes of the ER in cultured mammalian cells using a combination of quantitative confocal microscopy and EM as well as 3D modeling by ET.

Our ET analysis of interphase ER revealed that sheets were predominant over tubules in the central area of the cell, whereas peripheral areas close to plasma membrane had long interconnected tubules. Both confocal and thin section EM quantifications showed that mitotic ER profiles are shorter and more branched in comparison to interphase ER. The structural change explaining these results was revealed by ET of

mitotic ER: sheets were completely lost and transformed into branched tubular network.

These changes were correlated with the partitioning of the most pronounced subdomain of the ER, the NE, during mitosis. Studies concerning the partitioning of the NE at LM level have shown the spreading of the NE membrane proteins into and homogenous distribution within the ER network during mitosis (Ellenberg et al., 1997; Yang et al., 1997). Here, we confirm the redistribution of the inner nuclear membrane marker protein LBR-HRP into the ER network at the ultrastructural level, although the distribution of the label within the metaphase ER appeared somewhat more restricted than the almost homogenous distribution of the ssHRP-KDEL label (quantification data not depicted). We found frequent unstained tubules that were connected to stained ones. This may indicate that LBR is redistributed into distinct subdomains within the mitotic ER. The idea that NE building units would be kept as assembly-ready subdomains during mitosis is not completely new (Mattaj, 2004). However, we cannot make firm conclusions on this because the extent of HRP-induced staining depends heavily on the expression level of the protein. Fortunately, we were able to choose a low expressing cell line that does not induce NE invagination or membrane stacks, as reported in previous works (Ellenberg et al., 1997; Ma et al., 2007). Our estimations from Western blotting suggest that the total amount of LBR-HRP protein is approximately one third of the amount of ssHRP-KDEL protein (unpublished data). Whether this amount of protein could disperse and occupy the entire ER remains unanswered.

The structural changes of the ER from interphase sheets to highly branched tubular network after the onset of cell division is surprisingly radical and presumably requires the action of many molecular players. The first proteins involved in forming branch points and maintaining tubules have been found recently (for review see Shibata et al., 2006; Vedrenne and Hauri, 2006). Reticulons, especially the reticulon 4a (Rtn4a), and DP1, were suggested to function as tubule-forming hairpin proteins of the ER (Voeltz et al., 2006). Overexpression of Rtn4a abolished sheet structures from the interphase ER and created long, nonbranching tubules instead. Therefore, reticulon overexpression or relative abundance at the onset of cell division might explain the loss of sheets from the mitotic ER.

We were able to convert interphase ER sheets into highly branched tubules effectively mimicking the mitotic ER morphology by stripping the membrane-bound polysomes from the interphase ER with a puromycin treatment of cells. Similar treatment with cycloheximide that inhibits protein synthesis without causing the dissociation of ribosomes did not induce structural changes to the ER. Furthermore, quantification of ribosomes on ER membranes of interphase and mitotic cells revealed a major stripping of ribosomes during mitosis; prometaphase to anaphase cells had 70% decrease in ER-bound ribosomes compared to interphase cells. Quantification was done on each segment of transversely sectioned ER on random images and ribosomes were counted individually. We analyzed altogether 2.8 mm of ER membrane, and values obtained for interphase cells agree well with previous quantifications done on cultured interphase Buffalo Rat liver cells (Seiser and Nicchitta, 2000).

These results suggest that polysomes are involved in stabilizing sheet structures of the ER. The mechanism behind is unclear, but there are some interesting possibilities. One alternative introduced recently (Shibata et al., 2006) is that large polysomes might not fit on tubules with high membrane curvature; therefore polysomes must trigger formation of sheets. However, tubulation of ER was observed when the inhibition of translation by cycloheximide was prolonged to 2 h. While this treatment stripped a significant part of ribosomes from the ER, deprivation of some sheet stabilizing protein during the 2-h cycloheximide incubation, but not yet within the 15-min incubation, cannot be excluded.

Puromycin treatment splits the ribosome in half (Seiser and Nicchitta, 2000). Bound only by the 60S subunit, calcium has been shown to leak through the translocon (Roy and Wonderlin, 2003; Van Coppenolle et al., 2004). Because ER is the source for Ca^{2+} -signals during mitosis and mitotic progression is blocked if the signals are inhibited (Parry et al., 2005), the structural resemblance of the puromycin treated interphase ER to mitotic ER might be explained by the resemblance of the cytosolic Ca^{2+} environments. Interestingly, Ca^{2+} efflux from the ER has been shown to accompany also the ER network formation in *Xenopus* vesicles in vitro (Voeltz et al., 2006). A likely candidate responding to the Ca^{2+} efflux is the evolutionarily highly conserved p22 (Andrade et al., 2004) that promotes branching depending on cytoplasmic Ca^{2+} level.

Our results concerning the structural changes occurring during cell division are not in agreement with some of the earlier published work. In sea urchin embryos and *Xenopus* oocytes the ER remained continuous during mitosis, but accumulated at the mitotic poles (Terasaki, 2000; Terasaki et al., 2001). No obvious transformation from sheets to tubules was observed. In the early *Caenorhabditis elegans* embryo and *Drosophila melanogaster* syncytial embryos the ER forms sheets during mitosis and cycles between dispersed and accumulated states (Bobinnec et al., 2003; Poteryaev et al., 2005). These cell cycle–induced changes may reflect the rapid cell cycle and emphasis on partitioning of the NE. In this study, we have provided evidence that in cultured mammalian cells the abundant interphase ER structures, sheets, are lost and transform into a branched tubular network that remains continuous. The amount of ER-bound ribosomes is significantly reduced during the middle phases of mitosis. We propose that tubulation provides a simple, yet effective, mechanism for partitioning of the ER in cultured mammalian cells, and that the method to achieve these changes is linked to the ribosomal action on ER membranes—ribosomal stripping and inhibition of translation in the long run lead to loss of sheets and appearance of tubules both in interphase cells and during cell division.

Materials and methods

Cell culture and plasmids

CHO-K1 (CCL-61) cell line was cultured in DMEM containing 10% FBS, 1× non-essential amino acids, 10 mM Hepes buffer, and other supplements (all from Bio-Whittaker), and 100 μg/ml G418 (BD Biosciences), 180 μM puromycin-HCl (Sigma-Aldrich), or 180 μM cycloheximide (Sigma-Aldrich) when implicated. Transfections for the stable cell lines

were done with Fugene 6 (Roche). The CHO-K1/Hsp47-GFP cell line (Kano et al., 2005), pLBR-GFP (Ellenberg et al., 1997), and pssHRP-KDEL (Connolly et al., 1994) were provided by the respective laboratories. pLBR-HRP was created by cloning AgeI-HRP-NotI fragment with PCR into pLBR-GFP in place of the EGFP gene. Construction of pssGFP-KDEL is described elsewhere (Kuokkanen et al., 2007).

LM imaging

For quantification of the ER-bound S6 ribosomal protein, cells grown on 50 μg/ml fibronectin (Sigma-Aldrich)-coated coverslips were semi-permeabilized with 40 μg/ml digitonin (Seiser and Nicchitta, 2000), and cytosolic ribosomes were washed away with 1 M KCl for 2× 15 min on ice before fixation with PFA and immunostaining with S6-antibody (Jackson ImmunoResearch Laboratories). The cells were imaged with a UPlanApo 100×/1.35 (oil) objective in a wide-field AX70 Provis microscope using an F-View II CCD camera and AnalySIS software (Olympus) for 20 ms. The fluorescence intensity of S6 staining per cell was determined with ImagePro Plus 5.1 software (MediaCybernetics, Inc.).

For live-cell confocal imaging, cells were grown on fibronectin-coated glass-bottom dishes (MatTek). During imaging, the cells were kept in 40 mM Hepes-buffered growth medium at 37°C and 5 μM in vivo DNA stain DRAQ5 (Alexis Biochemicals) was added just before imaging when needed (Smith et al., 2000). For quantification, confocal image stacks were acquired with SP2 AOBS (Leica) using HCX PL APO 63×/1.2 W Corr/0.17 CS objective, red (HeNe 633 nm/10 mW) laser line for DRAQ5 and blue (Ar 488 nm/70 mW) for EGFP. The image stacks were collected through the cells and recorded by Leica confocal software, using parallel scanning, zoom 6, frame averaging 3 and 0.285-μm z-step. All stacks were deconvoluted with AutoQuant AutoDeblur 3D Blind deconvolution (Media Cybernetics, Inc.) using the same settings.

Imaging for co-compartmentalization analyses were done as above, but with HCX PL APO 63×/1.4–0.6 oil objective and lime laser (DPSS 561 nm/10 mW) for S6-staining using sequential scanning, 0.122-μm z-step and zoom 8. Deconvoluted stacks were analyzed with Imaris 5.7.1 Coloc tool using 5% threshold.

Quantification from confocal images

Every 2nd (interphase cells), 5th or 10th (mitotic cells) section through the confocal image stacks was analyzed, yielding an average of 3–4 sections or 4–5 sections per cell, respectively. A skeleton model of the ER network was formed with the branch and endpoint filter of ImagePro using thresholds 4–6 for CHO-K1/Hsp47-GFP and 4–20 for CHO-K1/ssGFP-KDEL depending on the brightness of individual cells. The cytoplasmic area containing ER and excluding areas devoid of ER was demarcated manually. This area, ER profile lengths, and branch points within the area were quantified with ImagePro. The resulting values from one cell were summed and related to the corresponding area, thus yielding an average value of the whole cell. Then, an average of all the cells within a mitotic phase was calculated.

To measure the volume where ER was confined, optical sections were chosen at regular intervals throughout the image stacks starting and ending with the top- and bottom-most sections of the cell. The ER area and ER-free areas, including the nucleus or chromosomes and the mitotic spindle, were traced by hand, digitized, and measured with ImagePro. The total volume with or without ER in the cell was then calculated by applying the Cavalieri principle (Gundersen and Jensen, 1987).

EM

For EM, cells grown on fibronectin-coated glass coverslips were cytochemically stained and flat embedded as described (Jokitalo et al., 2001). 80-nm-thick sections were cut parallel or perpendicular to the coverslip, post-stained with uranyl acetate and lead citrate, and observed with Tecnai 12 (FEI Corp.) operating at 80 kV. Images for quantification were acquired with ES500W CCD camera (Gatan Corp.) at 11,500× providing a pixel size of 6 nm. Cells for analysis were sampled randomly provided that their cell cycle phase could be reliably identified. The entire cellular profiles were imaged, and all stained ER profiles were traced manually by drawing the longest possible line from end to end along the middle of the profile onto transparencies, which were scanned and analyzed by ImagePro similarly to confocal images.

For ribosomal quantification, the cells were processed similarly, except that they were osmicated in non-reducing conditions and stained *en bloc* with 1% uranyl acetate, 0.3 M sucrose for 1.5 h at 4°C, and for data collection, the film camera of the microscope was used. ER membrane profiles of 60-nm sections at final magnification of 46,000× were traced along the transversely sectioned membranes. Ribosomes on them were counted individually and profile lengths were measured as above.

ET

For 3D ET, semi-thick (200 or 250 nm) sections were imaged with Tecnai FEG 20 (FEI Corp.) operating at 200 kV. Images for Figs. 6, 8, and 10 were collected with a 1k × 1k Multiscan 794 CCD camera (Gatan Corp.) at 3,500 or 5,000×, providing a pixel size of 5.42 nm or 3.68 nm, respectively, and for Fig. 2 with a 4k × 4k Ultrascan 4000 CCD camera (Gatan Corp.) at 5,000×, providing a 2× binned pixel size of 4.39 nm. For tilt series, the specimens were tilted at 1-degree intervals using a high tilt specimen holder (model 2020; E.A. Fischione Instruments) between ±65° or ±70°. Automated acquisition of the tilt series was carried out using either tomography software package provided by FEI Corp. or SerialEM software (Mastronarde, 2005). SerialEM enables automatic acquisition of montaged tilt series allowing tomography of larger areas, and by utilizing this feature, montages of 2 × 1, 3 × 1, or 2 × 2 frames were collected. For dual-axis tomography (Mastronarde, 1997), one tilt series was recorded from the area of interest, then the grid was rotated approximately 90° and a second tilt series from the same area was acquired.

The alignment of the tilt series was done with IMOD software package (Kremer et al., 1996) using 15-nm colloidal gold particles underneath or on top of the sections as fiducial markers. Tomographic reconstructions were analyzed and modeled with Amira (TGS Inc.). Before modeling the z-scale was elongated by the factor of 1.6 to compensate the compression of section by the electron beam.

Statistical analysis and image enhancements

Statistical significances of the differences between groups were calculated using single factor ANOVA in Excel 2003 (Microsoft). Contrast in images was enhanced by using the brightness and contrast tool of Adobe Photoshop 7.0.

Online supplemental material

Video 1 shows an animated model of a sheet-to-sheet branch from a 3D model of interphase ER shown in Fig. 6 A. Video 2 and Video 3 show z-series of the tomograms and 3D models of interphase and metaphase ER, respectively. Video 4 shows four dividing LBR-GFP/CHO-K1 cells and Fig. S1 still images of cell 3 of the video. Online supplemental material is available at http://www.jcb.org/cgi/content/full/jcb.200705112/DC1.

We thank Hisao Kondo for the CHO-K1/Hsp47-GFP cell line and Jan Ellenberg for the pLBR-GFP construct, Jussi Jäntti and Dave Shima for critical reading of the manuscript, Catherine Rabouille and Hisao Kondo for helpful discussion, Mervi Lindman for expert technical assistance in specimen preparation for ET, and the personnel of EM unit for technical support.

This work was funded by the Academy of Finland (projects 201198 and 115025) and University of Helsinki Research Funds. M. Puhka is a student of the Viikki Graduate School in Biosciences.

Submitted: 18 May 2007
Accepted: 5 November 2007

References

Andrade, J., H. Zhao, B. Titus, S. Timm Pearce, and M. Barroso. 2004. The EF-hand Ca2+-binding protein p22 plays a role in microtubule and endoplasmic reticulum organization and dynamics with distinct Ca2+-binding requirements. *Mol. Biol. Cell.* 15:481–496.

Bannykh, S.I., T. Rowe, and W.E. Balch. 1996. The organization of endoplasmic reticulum export complexes. *J. Cell Biol.* 135:19–35.

Baumann, O., and B. Walz. 2001. Endoplasmic reticulum of animal cells and its organization into structural and functional domains. *Int. Rev. Cytol.* 205:149–214.

Bobinnec, Y., C. Marcaillou, X. Morin, and A. Debec. 2003. Dynamics of the endoplasmic reticulum during early development of *Drosophila melanogaster*. *Cell Motil. Cytoskeleton.* 54:217–225.

Connolly, C.N., C.E. Futter, A. Gibson, C.R. Hopkins, and D.F. Cutler. 1994. Transport into and out of the Golgi complex studied by transfecting cells with cDNAs encoding horseradish peroxidase. *J. Cell Biol.* 127:641–652.

Dreier, L., and T.A. Rapoport. 2000. In vitro formation of the endoplasmic reticulum occurs independently of microtubules by a controlled fusion reaction. *J. Cell Biol.* 148:883–898.

Du, Y., S. Ferro-Novick, and P. Novick. 2004. Dynamics and inheritance of the endoplasmic reticulum. *J. Cell Sci.* 117:2871–2878.

Ellenberg, J., E.D. Siggia, J.E. Moreira, C.L. Smith, J.F. Presley, H.J. Worman, and J. Lippincott-Schwartz. 1997. Nuclear membrane dynamics and reassembly in living cells: targeting of an inner nuclear membrane protein in interphase and mitosis. *J. Cell Biol.* 138:1193–1206.

Geuze, H.J., J.L. Murk, A.K. Stroobants, J.M. Griffith, M.J. Kleijmeer, A.J. Koster, A.J. Verkleij, B. Distel, and H.F. Tabak. 2003. Involvement of the endoplasmic reticulum in peroxisome formation. *Mol. Biol. Cell.* 14:2900–2907.

Gundersen, H.J., and E.B. Jensen. 1987. The efficiency of systematic sampling in stereology and its prediction. *J. Microsc.* 147:229–263.

Jokitalo, E., N. Cabrera-Poch, G. Warren, and D.T. Shima. 2001. Golgi clusters and vesicles mediate mitotic inheritance independently of the endoplasmic reticulum. *J. Cell Biol.* 154:317–330.

Kano, F., H. Kondo, A. Yamamoto, Y. Kaneko, K. Uchiyama, N. Hosokawa, K. Nagata, and M. Murata. 2005. NSF/SNAPs and p97/p47/VCIP135 are sequentially required for cell cycle-dependent reformation of the ER network. *Genes Cells.* 10:989–999.

Kuokkanen, E., W. Smith, M. Mäkinen, H. Tuominen, M. Puhka, E. Jokitalo, S. Duvet, T. Berg, and P. Heikinheimo. 2007. Characterization and subcellular localization of human neutral class II α-mannosidase. *Glycobiology.* 17:1084–1093.

Kremer, J.R., D.N. Mastronarde, and J.R. McIntosh. 1996. Computer visualization of three-dimensional image data using IMOD. *J. Struct. Biol.* 116:71–76.

Le Breton, M., P. Cormier, R. Belle, O. Mulner-Lorillon, and J. Morales. 2005. Translational control during mitosis. *Biochimie.* 87:805–811.

Lee, C., and L.B. Chen. 1988. Dynamic behavior of endoplasmic reticulum in living cells. *Cell.* 54:37–46.

Levine, T., and C. Rabouille. 2005. Endoplasmic reticulum: one continuous network compartmentalized by extrinsic cues. *Curr. Opin. Cell Biol.* 17:362–368.

Lowe, M., and F.A. Barr. 2007. Inheritance and biogenesis of organelles in the secretory pathway. *Nat. Rev. Mol. Cell. Biol.* 8:429–439.

Ma, Y., S. Cai, Q. Lv, Q. Jiang, Q. Zhang, Sodmergen, Z. Zhai, and C. Zhang. 2007. Lamin B receptor plays a role in stimulating nuclear envelope production and targeting membrane vesicles to chromatin during nuclear envelope assembly through direct interaction with importin beta. *J.Cell. Sci.* 120:520–530.

Mastronarde, D.N. 1997. Dual-axis tomography: an approach with alignment methods that preserve resolution. *J. Struct. Biol.* 120:343–352.

Mastronarde, D.N. 2005. Automated electron microscope tomography using robust prediction of specimen movements. *J. Struct. Biol.* 152:36–51.

Mattaj, I.W. 2004. Sorting out the nuclear envelope from the endoplasmic reticulum. *Nat. Rev. Mol. Cell Biol.* 5:65–69.

McCullough, S., and J. Lucocq. 2005. Endoplasmic reticulum positioning and partitioning in mitotic HeLa cells. *J. Anat.* 206:415–425.

Nagata, K. 1998. Expression and function of heat shock protein 47: a collagen-specific molecular chaperone in the endoplasmic reticulum. *Matrix Biol.* 16:379–386.

Papp, S., E. Dziak, M. Michalak, and M. Opas. 2003. Is all of the endoplasmic reticulum created equal? The effects of the heterogeneous distribution of endoplasmic reticulum Ca2+-handling proteins. *J. Cell Biol.* 160:475–479.

Parry, H., A. McDougall, and M. Whitaker. 2005. Microdomains bounded by endoplasmic reticulum segregate cell cycle calcium transients in syncytial *Drosophila* embryos. *J. Cell Biol.* 171:47–59.

Poteryaev, D., J.M. Squirrell, J.M. Campbell, J.G. White, and A. Spang. 2005. Involvement of the actin cytoskeleton and homotypic membrane fusion in ER dynamics in *Caenorhabditis elegans*. *Mol. Biol. Cell.* 16:2139–2153.

Rizzuto, R., M.R. Duchen, and T. Pozzan. 2004. Flirting in little space: the ER/mitochondria Ca2+ liaison. *Sci. STKE.* 2004:re1.

Robenek, M.J., N.J. Severs, K. Schlattmann, G. Plenz, K.P. Zimmer, D. Troyer, and H. Robenek. 2004. Lipids partition caveolin-1 from ER membranes into lipid droplets: updating the model of lipid droplet biogenesis. *FASEB J.* 18:866–868.

Roy, A., and W.F. Wonderlin. 2003. The permeability of the endoplasmic reticulum is dynamically coupled to protein synthesis. *J. Biol. Chem.* 278:4397–4403.

Scharff, M.D., and E. Robbins. 1966. Polyribosome disaggregation during metaphase. *Science.* 151:992–995.

Seiser, R.M., and C.V. Nicchitta. 2000. The fate of membrane-bound ribosomes following the termination of protein synthesis. *J. Biol. Chem.* 275:33820–33827.

Shibata, Y., G.K. Voeltz, and T.A. Rapoport. 2006. Rough sheets and smooth tubules. *Cell.* 126:435–439.

Sitia, R., and J. Meldolesi. 1992. Endoplasmic reticulum: a dynamic patchwork of specialized subregions. *Mol. Biol. Cell.* 3:1067–1072.

Smith, P.J., N. Blunt, M. Wiltshire, T. Hoy, P. Teesdale-Spittle, M.R. Craven, J.V. Watson, W.B. Amos, R.J. Errington, and L.H. Patterson. 2000. Characteristics of a novel deep red/infrared fluorescent cell-permeant DNA probe, DRAQ5, in intact human cells analyzed by flow cytometry, confocal and multiphoton microscopy. *Cytometry.* 40:280–291.

Snapp, E.L., R.S. Hegde, M. Francolini, F. Lombardo, S. Colombo, E. Pedrazzini, N. Borgese, and J. Lippincott-Schwartz. 2003. Formation of stacked ER cisternae by low affinity protein interactions. *J. Cell Biol.* 163:257–269.

Staehelin, L.A. 1997. The plant ER: a dynamic organelle composed of a large number of discrete functional domains. *Plant J.* 11:1151–1165.

Terasaki, M. 2000. Dynamics of the endoplasmic reticulum and Golgi apparatus during early sea urchin development. *Mol. Biol. Cell.* 11:897–914.

Terasaki, M., L.L. Runft, and A.R. Hand. 2001. Changes in organization of the endoplasmic reticulum during *Xenopus* oocyte maturation and activation. *Mol. Biol. Cell.* 12:1103–1116.

Uchiyama, K., E. Jokitalo, F. Kano, M. Murata, X. Zhang, B. Canas, R. Newman, C. Rabouille, D. Pappin, P. Freemont, and H. Kondo. 2002. VCIP135, a novel essential factor for p97/p47-mediated membrane fusion, is required for Golgi and ER assembly in vivo. *J. Cell Biol.* 159:855–866.

Van Coppenolle, F., F. Vanden Abeele, C. Slomianny, M. Flourakis, J. Hesketh, E. Dewailly, and N. Prevarskaya. 2004. Ribosome-translocon complex mediates calcium leakage from endoplasmic reticulum stores. *J. Cell Sci.* 117:4135–4142.

Vedrenne, C., and H.P. Hauri. 2006. Morphogenesis of the endoplasmic reticulum: beyond active membrane expansion. *Traffic.* 7:639–646.

Voeltz, G.K., M.M. Rolls, and T.A. Rapoport. 2002. Structural organization of the endoplasmic reticulum. *EMBO Rep.* 3:944–950.

Voeltz, G.K., W.A. Prinz, Y. Shibata, J.M. Rist, and T.A. Rapoport. 2006. A class of membrane proteins shaping the tubular endoplasmic reticulum. *Cell.* 124:573–586.

Warren, G., and W. Wickner. 1996. Organelle inheritance. *Cell.* 84:395–400.

Waterman-Storer, C.M., and E.D. Salmon. 1998. Endoplasmic reticulum membrane tubules are distributed by microtubules in living cells using three distinct mechanisms. *Curr. Biol.* 8:798–806.

Wollert, T., D.G. Weiss, H.H. Gerdes, and S.A. Kuznetsov. 2002. Activation of myosin V-based motility and F-actin-dependent network formation of endoplasmic reticulum during mitosis. *J. Cell Biol.* 159:571–577.

Yang, L., T. Guan, and L. Gerace. 1997. Integral membrane proteins of the nuclear envelope are dispersed throughout the endoplasmic reticulum during mitosis. *J. Cell Biol.* 137:1199–1210.

Zeligs, J.D., and S.H. Wollman. 1979. Mitosis in rat thyroid epithelial cells in vivo. I. Ultrastructural changes in cytoplasmic organelles during the mitotic cycle. *J. Ultrastruct. Res.* 66:53–77.